



# Experimental and Numerical Investigation on Interaction Mechanism Between Hydraulic Fracture and Natural Fracture

Haifeng Fu<sup>1,2</sup> · Liuke Huang<sup>3</sup> · Bing Hou<sup>1,4</sup> · Dingwei Weng<sup>2</sup> · Baoshan Guan<sup>2</sup> · Taixian Zhong<sup>5</sup> · Yulong Zhao<sup>6</sup>

Received: 5 March 2024 / Accepted: 25 July 2024

© The Author(s), under exclusive licence to Springer-Verlag GmbH Austria, part of Springer Nature 2024

## Abstract

Hydraulic fracture propagation under natural fracture distributions has always been a hot topic in unconventional reservoir stimulation. In this work, the hydromechanical behavior controlled by rock fabric is understood and quantified via physical and numerical simulations. A unique large-scale (762 mm × 762 mm × 914 mm) hydraulic fracturing simulation experimental technology considering quantitative simulation of the cementation performance of natural fractures is established. Combined with the laboratory results, a planar, heterogeneous, multiscale hydraulic fracturing numerical model based on the cohesive zone method is developed and verified. The experimental and numerical results reveal three simple modes between hydraulic fracture and natural fracture, namely, natural fracture opening, shearing and crossing. In addition, some mixed modes of complex fracture exist. Compared with engineering factors, the interaction between natural fractures and hydraulic fractures is more obviously controlled by geological factors. A greater horizontal stress difference, angle between the maximum horizontal stress direction and natural fracture, tensile strength of natural fractures and pumping parameters are conducive to crossing natural fractures. On the basis of the simulation results, three field-scale diagrams of the interaction between natural fractures and hydraulic fractures are systematically established. The interaction results can be visualized in reference to most geological and engineering conditions. Considering the greater horizontal stress difference and natural underdevelopment, the single model of fracture propagation along the maximum direction is dominant in most tight or shale oil basins in China. The physical and numerical simulation technologies in this paper will help to optimize the volume stimulation design of unconventional reservoirs.

## Highlights

- A unique large-scale hydraulic fracturing simulation experimental technology considering quantitative simulation of the cementation performance of natural fractures is established
- Three field-scale diagrams of the interaction between natural fracture and hydraulic fracture are established systematically
- Revealing the interaction mechanism between hydraulic fracture and natural fracture

**Keywords** Hydraulic fracturing · Natural fracture · Large-scale experiment · Numerical modeling · Unconventional reservoir

✉ Liuke Huang  
swpuhik@126.com

<sup>1</sup> College of Petroleum Engineering, China University of Petroleum, Beijing 102249, China

<sup>2</sup> Research Institute of Petroleum Exploration and Development, PetroChina, Beijing 100083, China

<sup>3</sup> School of Civil Engineering and Geomatics, Southwest Petroleum University, Chengdu 610500, Sichuan, China

<sup>4</sup> National Key Laboratory of Petroleum Resource and Engineering, China University of Petroleum, Beijing 102249, China

<sup>5</sup> CNPC Science and Technology Management Department, Beijing 100007, China

<sup>6</sup> National Key Laboratory of Oil and Gas Reservoir Geology and Exploitation, Southwest Petroleum University, Chengdu 610500, China

## 1 Introduction

Hydraulic fracturing has become a key engineering technology in unconventional development, and the fracturing process design has transformed from traditional single and high-conductivity fractures into complex fracture networks and low-conductivity fractures (Huang et al. 2023a; Niu et al. 2022; Tan et al. 2023; Wu et al. 2023). Mine fracturing tests clearly demonstrate the complexity of hydraulic fracture configurations for the first time and have begun to shake the traditional classical theory of single-winged symmetrical fractures (Warpinski et al. 1993; Warpinski and Teufel 1987). The large-scale sliced-water fracturing technique in the Barnett Basin has enabled commercial shale gas mines for the first time, and microseism technology first confirmed the existence of complex fracture networks in shale gas reservoirs (Fisher et al. 2005, 2004). As a result of the communication between natural fractures and hydraulic fractures, the reservoir movement effect is greatly improved. On the basis of the above understanding, volume reconstruction design for the purpose of "maximizing reservoir contact area" has gradually become the mainstream stimulation technology in unconventional reservoir development (Hu et al. 2018; Huang et al. 2023b; Liu et al. 2023; Niu et al. 2021; Tan et al. 2024a, b; Song et al. 2017, 2020). Among them, how to create complex fracture networks and realize the maximum communication between natural fractures and hydraulic fractures has become the key to process optimization and the focus of basic research.

Laboratory testing is important for studying hydraulic fracturing. Scholars have conducted experimental research on hydraulic fracturing under natural fracture conditions, with rock samples of different scales (10–100 cm) and different shapes (cylindrical, cubic) (Huang et al. 2024; Ishibashi et al. 2023; Llanos et al. 2017; Mao et al. 2017; Zhang et al. 2021, 2023). Focusing on the natural fracture trend, in-situ stress conditions, and influence of construction parameters on hydraulic fracture morphology, qualitative or quantitative research has been conducted, revealing the general rule of hydraulic fracture. However, experimental research has not yet reached the degree of complete quantification, in particular, the simulation of natural fracture performance and strength is still in the stage of qualitative understanding due to the restrictions of the experimental scale and experimental technology level.

Numerical simulation is an important method for studying hydraulic fracturing (Huang et al. 2018, 2019; Li et al. 2020, 2024a; Zhang et al. 2019, 2022a). In terms of numerical simulation, Zhang et al. used the displacement discontinuity method (DDM) to simulate the deflection and growth of hydraulic fractures on a rock surface (Chen et al. 2019; Weng et al. 2011; Zhang et al. 2007,

2017). The extended finite element method is an effective method for simulating the interaction between hydraulic fractures and natural fractures (Arash and Olson 2011; Li et al. 2023; Tan et al. 2021; Zhang et al. 2022b). The effects of in-situ stress, the fracture phase angle and the degree of fracture cementation on fracture growth are investigated via the cohesive zone method, which is based on the finite element method (Guo et al. 2015; Li et al. 2024b; Pidho et al. 2023). In addition, the two-dimensional continuous discrete mixing numerical method, block discrete element method, particle discrete element method, and three-dimensional lattice method are used to simulate the crossing of hydraulic fracturing fractures at single or multiple natural fracture interfaces, and the influences of multiple factors, such as in-situ stress, material heterogeneity, fracturing fracture properties and pumping parameters, on the crossing process are studied (He et al. 2023; Huang et al. 2020, 2022; Zhang and Mack 2017; Zheng et al. 2022). Major numerical simulation research has been carried out by predecessors, however, considering the stability and efficiency of the calculation, more analytic solution methods have been adopted to study the interaction between natural fracture and hydraulic fracture. In fact, real-time force calculations near natural cracks are not realized. Moreover, the simulation results are not combined with physical model experiments in an effective way and the combination accuracy remains to be verified and improved.

Taking large-scale natural fractures into consideration, a fracturing simulation experiment technique is established on the basis of experimental method innovation in this paper. This study contributes to the realization of quantitative simulations of the properties of natural fracture cementation. Combined with the experimental results, a plane, heterogeneous and multiscale numerical model of hydraulic fracturing is established on the basis of the cohesive zone method. Quantitative analysis of the influence of the horizontal stress difference, natural fracture dip angle, natural fracture tensile strength and construction parameters at the field scale on the interaction between natural fractures and hydraulic fractures was performed. Formation of the role of the chart helps with onsite unconventional reservoir volume reconstruction process inventions and provides the most direct and effective means of design optimization.

## 2 Physical Simulation

### 2.1 The Principle of Experimental Design

A dimensionless analysis method based on similarity theory was established to design experimental parameters for

hydraulic fracturing (De Pater et al. 1994; Luo et al. 2022). To achieve geometric rock deformation, fluid flow and boundary condition similarities between the laboratory scale and the field scale, a sample should have extremely low fracture toughness and low permeability, and high viscosity fluids or appropriate injection rates should be adopted to minimize the effects of rock toughness. However, owing to limitations in the capacity of laboratory equipment, satisfying the above requirements in practice is difficult. Therefore, Detournay introduces the characteristic number  $K$  (a dimensionless toughness) in Eq. 1 to describe the similarity in fracture propagation (Detournay 2004, 2016). For  $K < 1$ , the energy dissipation during fracture propagation mainly depends on the fluid rate (viscosity). For  $K > 4$ , the main controlling factor of energy dissipation is rock fracture toughness. For  $1 < K < 4$ , fracture propagation transitions from the viscosity-dominated regime to the toughness-dominated regime. Since viscosity is often the dominant factor during hydraulic fracturing field operation, reasonable values should be assigned to injection parameters in laboratory experiments to realistically mimic the viscosity-dominated regime of hydraulic fracture propagation in the field (Dontsov 2016, 2022a, b):

$$K = 4 \left( \frac{2}{\pi} \right)^{\frac{1}{2}} K_{IC} \left( \frac{t^2}{Q^3 (E / (1 - \nu^2))^{13} (12\mu)^5} \right)^{\frac{1}{18}} \quad (1)$$

where  $E$  is the Young's modulus (MPa) of the reservoir;  $\mu$  is the Poisson's ratio of the reservoir; and  $K_{IC}$  is the fracture toughness (MPa $\cdot\sqrt{m}$ ) of the reservoir.

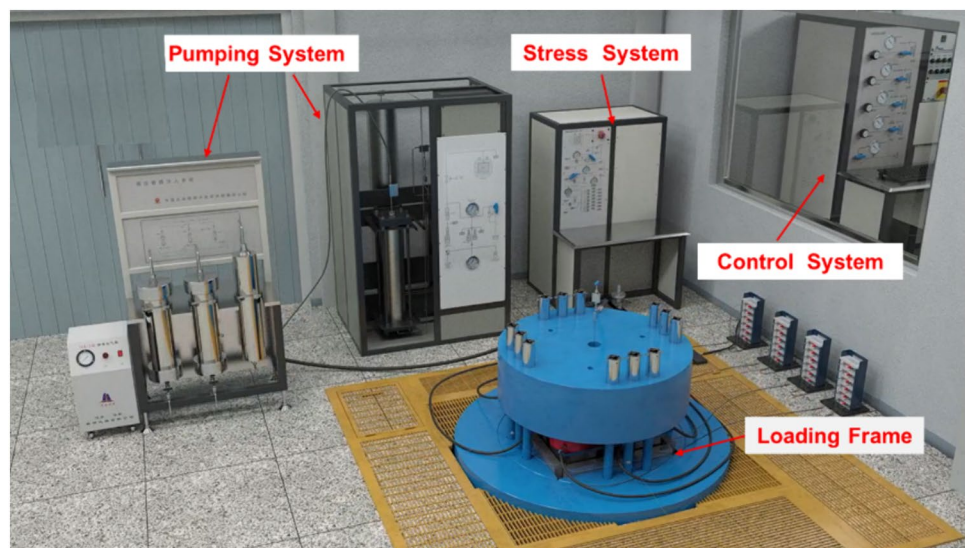
## 2.2 Validation of the Numerical Method

In this study, a large-scale full 3D physical simulation experiment system for hydraulic fracturing is applied, as shown in Fig. 1 (Fu et al. 2021). This system consists of

four parts: the rock-sample loading frame, the stress system, the automatic control system for data acquisition, and the pumping system. The size of the test rock sample is 762 mm  $\times$  762 mm  $\times$  914 mm, which is the largest for fracturing experiments in the world. When a rock sample is large, the boundary effect can be effectively reduced, and simulations of steady fracture propagation are more closely related to field situations. In the experimental system, special flexible loading plates instead of traditional rigid jacks can be designed to load in situ stresses. The maximum level can reach 69 MPa.

The existence of natural fractures and horizontal bedding is a typical unconventional reservoir geological characteristic. Therefore, studies on the mechanism of hydraulic fracturing considering natural fractures have always been popular. Owing to the mechanical properties of natural samples and the randomness of their natural distribution, quantitative and repetitive research is difficult. In this work, artificial samples could be used to control rock mechanics. One special material called mesh fiberglass is prefabricated to simulate a natural weak surface. The mesh material has two unique advantages: the weak surface has a certain permeability, and the bonding strength of the weak surface can be quantitatively simulated according to the different mesh sizes of the material. An experimental device for variable angle shear testing is developed, which can obtain strength parameters such as the cohesion force and internal friction angle of a weak surface, and provide reliable experimental technical support for the establishment of a numerical model. Figure 2 shows the test results for two different weak surface bonding strengths, and the relationship between normal stress and shear stress in shear test is approximately linear. The friction coefficient of prefabricated natural fractures in the experiments is 0.8816, and the bond strength is 0.7842 MPa.

**Fig. 1** Vertical view of the horizontal stress of the loading layer



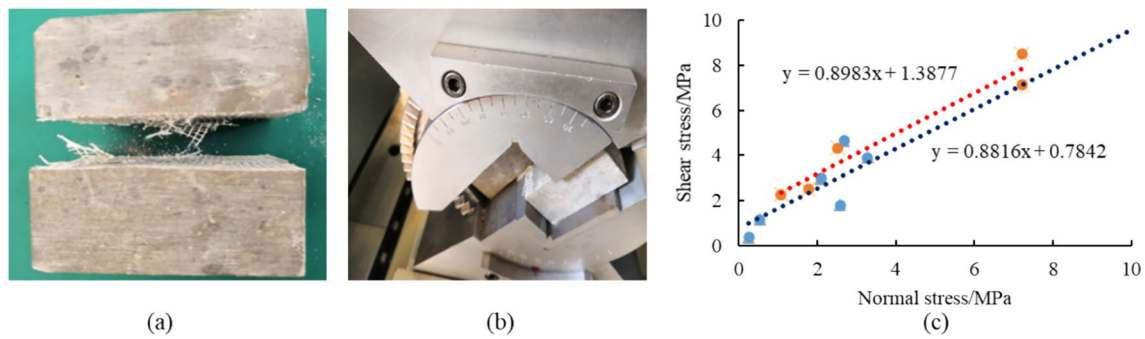


**Fig. 2** Test methods for natural fracture simulation and mechanical performance evaluation, **(a)** artificial weakness plane, **(b)** shear testing device, and **(c)** relationship curve between normal stress and shear stress for shear testing results of two weak planes

### 2.3 Experimental Results

Considering the existence of natural fractures, many factors affect hydraulic fracture propagation. To investigate more factors with a limited number of experiments, this paper uses the orthogonal design method and performs a total of nine groups of experiments with four factors and three levels. The sensitivity of the injection rate, viscosity, angle and horizontal stress difference to fracture height extension is analysed. The specific experimental parameters and results are shown in Table 1. In the simulation of vertical well fracturing, the vertical stress (along the direction of the wellbore) is the maximum principal stress ( $\sigma_v$ ) of 20 MPa, the minimum horizontal principal stress ( $\sigma_h$ ) is 10 MPa, and the maximum horizontal principal stress ( $\sigma_H$ ) is 12 MPa, 15 MPa and 18 MPa. All of the prefabricated natural fractures are vertical. The angles between the direction of natural fracture and the direction of the maximum horizontal principal stress are set to 30°, 60° and 90°. At the same time, combined with the injection capacity of the experimental equipment, the injection rate and fluid viscosity are set to three different values which are listed in Table 1.

After the experiments, the rock samples were removed for dissection to observe the actual fracture morphology. The rock samples are digitized via 3D laser scanning to display the fracture morphology in 3D space. Figure 3 shows some of the experimental results. As the angle between natural fractures and the maximum principal stress decreases, natural fractures tend to open. For example, when the angle is 90°, all three experiments pass through natural fractures; when the angle is decreased to 60°, one experiment opens natural fractures; and when the angle is decreased to 30°, all three experiments open natural fractures. As the horizontal stress difference increases, hydraulic fractures tend to propagate through natural fractures. For example, when the horizontal stress difference is 2 MPa, only one experiment passes through the natural fracture, whereas under horizontal stress differences of 5 MPa and 8 MPa, two experiments pass

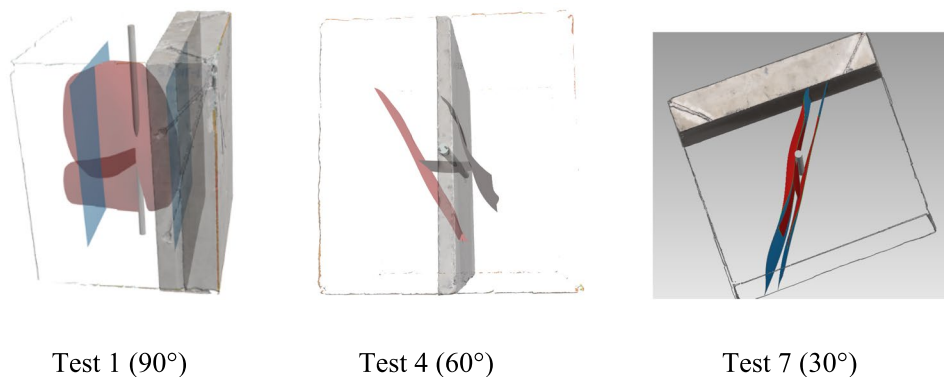
**Table 1** Experimental scheme and results of hydraulic fracturing with prefabricated fractures

Test	Angle/°	Horizontal Stress Difference/MPa	Injection rate/ $\text{cm}^3 \cdot \text{min}^{-1}$	Viscosity/cp	Results
1	90	2	60	5	Crossing
2	90	5	120	20	Crossing
3	90	8	240	50	Crossing
4	60	2	120	50	Opening
5	60	5	240	5	Crossing
6	60	8	60	20	Crossing
7	30	2	240	20	Opening
8	30	5	60	50	Opening
9	30	8	120	5	Opening

through natural fractures. On the other hand, the influence of the pumping parameters on fracture propagation does not exhibit an obvious trend. Two experiments involved crossing natural fractures at a low injection rate of 60 ml/min, one experiment involved crossing natural fractures at 120 ml/min, and two experiments involved crossing natural fractures at 240 ml/min. However, under the condition of high viscosity liquid injection, the trend of natural fracture opening is more obvious, which contradicts the general understanding and should be related to other experimental conditions.

Compared with engineering factors, geological conditions have a more significant influence on the interaction between hydraulic fracture and natural fracture. A lower angle of natural fractures and horizontal stress differences

**Fig. 3** 3D fracture geometry of the fracturing test



are conducive to the opening of natural fractures. Although only nine experiments have been carried out, which can provide only a qualitative understanding, they can still provide more reliable technical support for the subsequent numerical model establishment and optimization.

### 3 Numerical Simulation

#### 3.1 Technology Introduction

On the basis of cohesive force element technology in the finite element method and the theory of hydraulic fracture propagation, a two-dimensional hydraulic fracture propagation simulation program considering natural fractures is written in the finite element software ABAQUS with FORTRAN, which can simulate hydraulic fracture propagation and the interaction between hydraulic fractures and natural fractures. In this model, we assume that the fracture is always vertical (in most non-shallow reservoir conditions, the vertical stress is always the maximum principal stress, so this assumption is always satisfied), but can extend in any horizontal direction. The fracture consists of a series of structured rectangular elements, with the main variables (such as pressure and crack width) located at the central node of the edge in the direction of the thickness of the element. The vertical fracture element dimensions can be automatically adjusted to match the thicknesses of different layers accurately, whereas the horizontal fracture element dimensions can be matched with the surrounding rock matrix elements to improve the computational efficiency.

Specifically, a failure criterion containing a linear softening section is used to define the cohesive force element, which requires two material parameters to describe the propagation of the fracture: fracture energy  $G_c$  (calculated from Young's modulus  $E$  and fracture toughness  $K_{IC}$ ), and maximum tensile force  $N_0$ , as shown in Fig. 4. In the cohesive force element, it is necessary to define the behavior of the tension and fracture width before the fracture is fully opened and destroyed, which is assumed here as a linear relationship

determined by the initial stiffness  $K_0$ . This criterion can be regarded as a generalized irreversible cohesion criterion for the linear reduction in initial stiffness and is widely used in fracture failure simulations of brittle materials. In Fig. 4, the tension of the cohesive force unit decreases linearly from the maximum strength  $N_0$  at the time of damage initiation to 0. When the crack opening displacement exceeds the critical width  $w_1$ , no cohesive force is generated, the unit is completely disconnected and the crack expands forwards. If the element is unloaded before the fracture completely damaged, the cohesion of the crack decreases along the damaged stiffness  $K_p$ , which can be expressed as

$$N = K_p w, \quad 0 \leq w \leq w_p \tag{2}$$

where  $N$  is the fracture surface tension,  $w$  is the fracture width, and  $w_p$  is the historical maximum fracture width of the crack at the unit. After fracture damage initiation, the surface of a natural fracture will be subjected to fluid pressure  $p$ , so the total tension of the fracture surface is as follows:

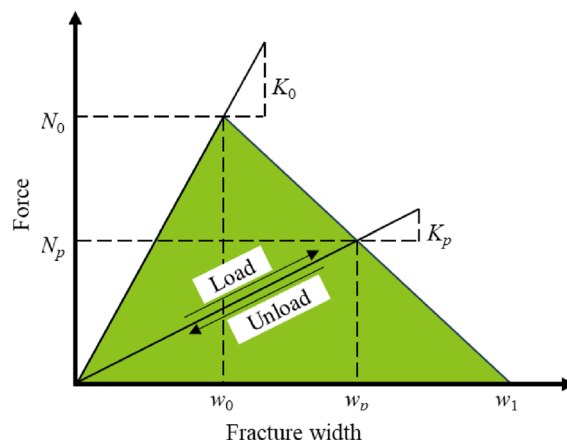


**Fig. 4** Failure criterion of cohesive element (fracture propagation criterion)

**Table 2** Basic parameters of numerical models for multiple scales

Model	Model size/m	$\sigma_h$ /MPa	Tensile strength $\sigma_t$ /MPa	$K_{IC}$ / MPa·m <sup>0.5</sup>	Young's modulus/MPa	Poisson's ratio
Lab	0.762×0.762	10	3	1	15,000	0.2
Field	1,000,800	60	3	1	30,000	0.2

$$N = K_p w - p, \quad 0 \leq w \leq w_p \tag{3}$$

The fluid flow in the fracture satisfies the mass conservation equation:

$$\frac{\partial w}{\partial t} = \frac{\partial q_x}{\partial x} + \frac{\partial q_y}{\partial y} + q_i - q_l \tag{4}$$

where  $w$  is the crack width,  $q_l$  is the leak off flow rate, and  $q_i$  is the injection rate. The momentum equation of fluid movement is

$$q_x = -\frac{n}{2n+1} 2^{-\frac{n+1}{n}} w^{\frac{2n+1}{n}} K^{-\frac{1}{n}} \left[ \left( \frac{\partial p}{\partial x} + \rho g_x \right)^2 + \left( \frac{\partial p}{\partial y} + \rho g_y \right)^2 \right]^{\frac{1-2n}{2n}} \left( \frac{\partial p}{\partial x} + \rho g_x \right) \tag{5}$$

$$q_y = -\frac{n}{2n+1} 2^{-\frac{n+1}{n}} w^{\frac{2n+1}{n}} K^{-\frac{1}{n}} \left[ \left( \frac{\partial p}{\partial x} + \rho g_x \right)^2 + \left( \frac{\partial p}{\partial y} + \rho g_y \right)^2 \right]^{\frac{1-2n}{2n}} \left( \frac{\partial p}{\partial y} + \rho g_y \right)$$

where  $q_x$  and  $q_y$  are the flows in the directions of  $x$  and  $y$ , respectively.  $g_x$  and  $g_y$  are the components of gravitational acceleration in the directions of  $x$  and  $y$ , respectively.  $p$  is the fluid pressure. Where  $\rho$  is the density of the sand-carrying fluid.  $n$  and  $K$  are the power law index and power law coefficient of the power law fluid, respectively. Carter one-dimensional fluid loss model is used for fluid loss:

$$q_l = \frac{2C_L}{\sqrt{t - \tau(x, y)}} \tag{6}$$

where  $\tau(x, y)$  is the time at which the fracturing fluid arrives at the fracture surface, and  $C_L$  is the leak off coefficient.

### 3.2 Model Validation

The greatest advantage of this numerical simulation technology is that it is not restricted by the model scale, from the laboratory scale to the field scale. Moreover, the stress field during the fracture propagation can also be calculated in real time. Using the criterion of tensile stress damage and the Mohr–Coulomb criterion, the failure of the matrix or natural fracture can be judged in real time. The calculation accuracy is guaranteed. The idea of this study is to establish the experimental scale model firstly, and conduct the correction and optimization based on the previous experimental data. Furthermore, an onsite scale model is then established to guide the process design optimization. By adjusting the mesh size

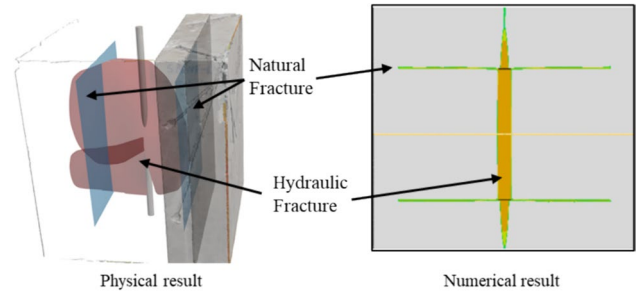


**Fig. 5** Comparison between the physical and numerical results of the No. 1 test

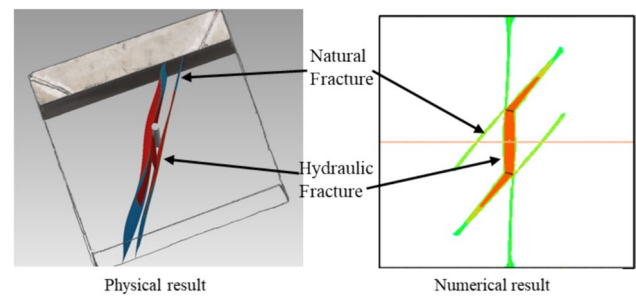


**Fig. 6** Comparison between the physical and numerical results of the No. 7 test

of the numerical model and the mechanical parameters, pumping pressure curve fitting between the physical and numerical models can be realized. The basic parameters of the model are shown in Table 2, and a comparison between the numerical and experimental results is shown in Figs. 5 and 6. The hydraulic fracturing results of the two tests are consistent.

### 3.3 Simulation Results

According to the literature and experimental analysis, the main geological factors affecting hydraulic fracture propagation are the natural fracture mechanical performance (tensile strength, cohesion, and internal friction angle), the natural fracture angle and the horizontal stress difference. Moreover, a total of six influencing factors are investigated considering three engineering parameters, namely, the injection rate, fluid viscosity and fluid volume. In this study, each factor is set to two, three, or five levels to carry

**Table 3** Basic parameters of the numerical simulation at the field scale

Natural fracture tensile strength $T_n$ /MPa	Natural fracture angle $\theta/^\circ$	Horizontal stress difference $\Delta\sigma$ /MPa	Injection rate $Q_0 / \text{m}^3 \cdot \text{min}^{-1}$	Fluid viscosity $\mu/\text{cp}$	Fluid volume per fracture $V_p / \text{m}^3$
0.5, 1, 1.5	30, 60, 90	0, 1, 2, 3, 4, 5	3, 15	5, 50	200, 300

out the field scale simulation, as shown in Table 3. The internal friction angle is fixed at  $40^\circ$  to reduce the number of computations. The natural fracture cohesion and tensile strength are set to the same values. Therefore, a total of 432 numerical groups were calculated.

A series of two-dimensional charts are drawn via the numerical simulation. Figures 7–10 show that as the mechanical strength of a natural fracture mechanical strength increases (from left to right), the area of hydraulic fracture crossing a natural fracture expands. The smaller

the angle between natural fractures and hydraulic fractures is, the greater the horizontal two-phase principal stress difference, and the more conducive the opening of natural fractures is. When the injection rate increases, the area of hydraulic fracture crossing further expands, which is conducive to creating a simple fracture system. As shown in Fig. 8, when the dip angle is reduced to  $30^\circ$  and the horizontal stress difference is 4 MPa, hydraulic fractures can still propagate directly through natural fractures. When the fluid viscosity decreases, the area of natural fracture opening further expands, which is conducive to the communication of natural fractures, as shown in Fig. 9. At this time, the angle is the dominant geological factor. Once it is less than  $30^\circ$ , the natural fracture remains open without being affected by other factors. When the volume of the pumping fluid is further increased, the interaction between natural fractures and hydraulic fractures does not change significantly. However, in terms of the stimulation reservoir volume, increasing of the fluid volume increased the fracture propagation scale, and the treatment pressure also increased slightly.

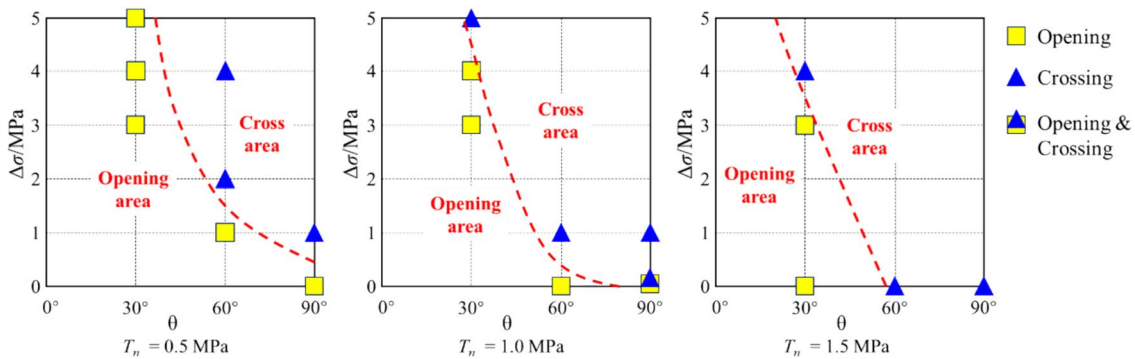


**Fig. 7** Diagram of the interactions between the hydraulic fracture and the natural fracture for  $Q_0=3 \text{ m}^3/\text{min}$ ,  $\mu=50 \text{ cp}$ ,  $V_p=200 \text{ m}^3$  ( $\Delta\sigma$  is the horizontal two-phase principal stress difference, and  $\theta$  is the angle between natural fracture and maximum horizontal stress)

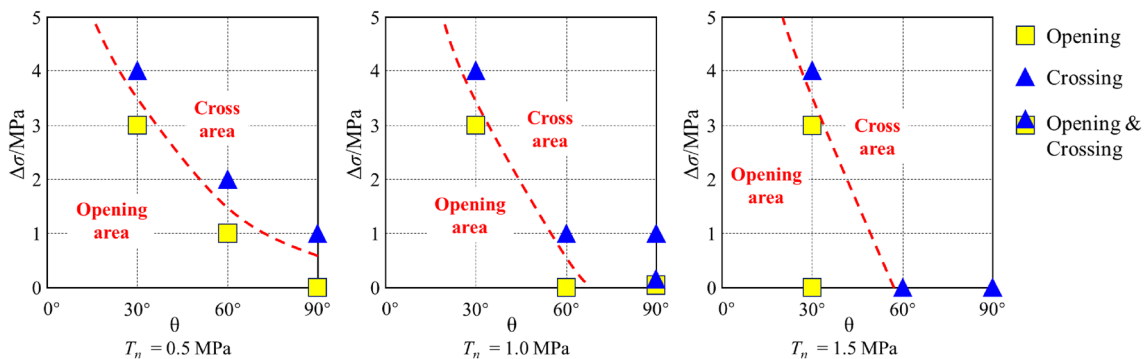


**Fig. 8** Diagram of the interactions between the hydraulic fracture and the natural fracture for  $Q_0=15 \text{ m}^3/\text{min}$ ,  $\mu=50 \text{ cp}$ , and  $V_p=200 \text{ m}^3$  ( $\Delta\sigma$  is the horizontal two-phase principal stress difference, and  $\theta$  is the angle between the natural fracture and the maximum horizontal stress)

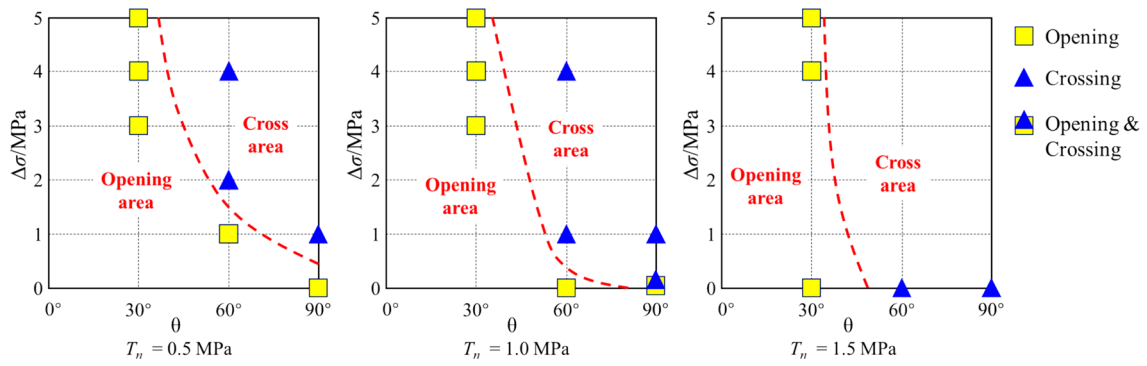


**Fig. 9** Diagram of the interactions between the hydraulic fracture and the natural fracture for  $Q_0=15 \text{ m}^3/\text{min}$ ,  $\mu=5 \text{ cp}$ , and  $V_p=200 \text{ m}^3$ . As the fluid continues to be injected to  $300 \text{ m}^3$ , the interaction results

remain the same ( $\Delta\sigma$  is the horizontal two-phase principal stress difference, and  $\theta$  is the angle between the natural fracture and the maximum horizontal stress)

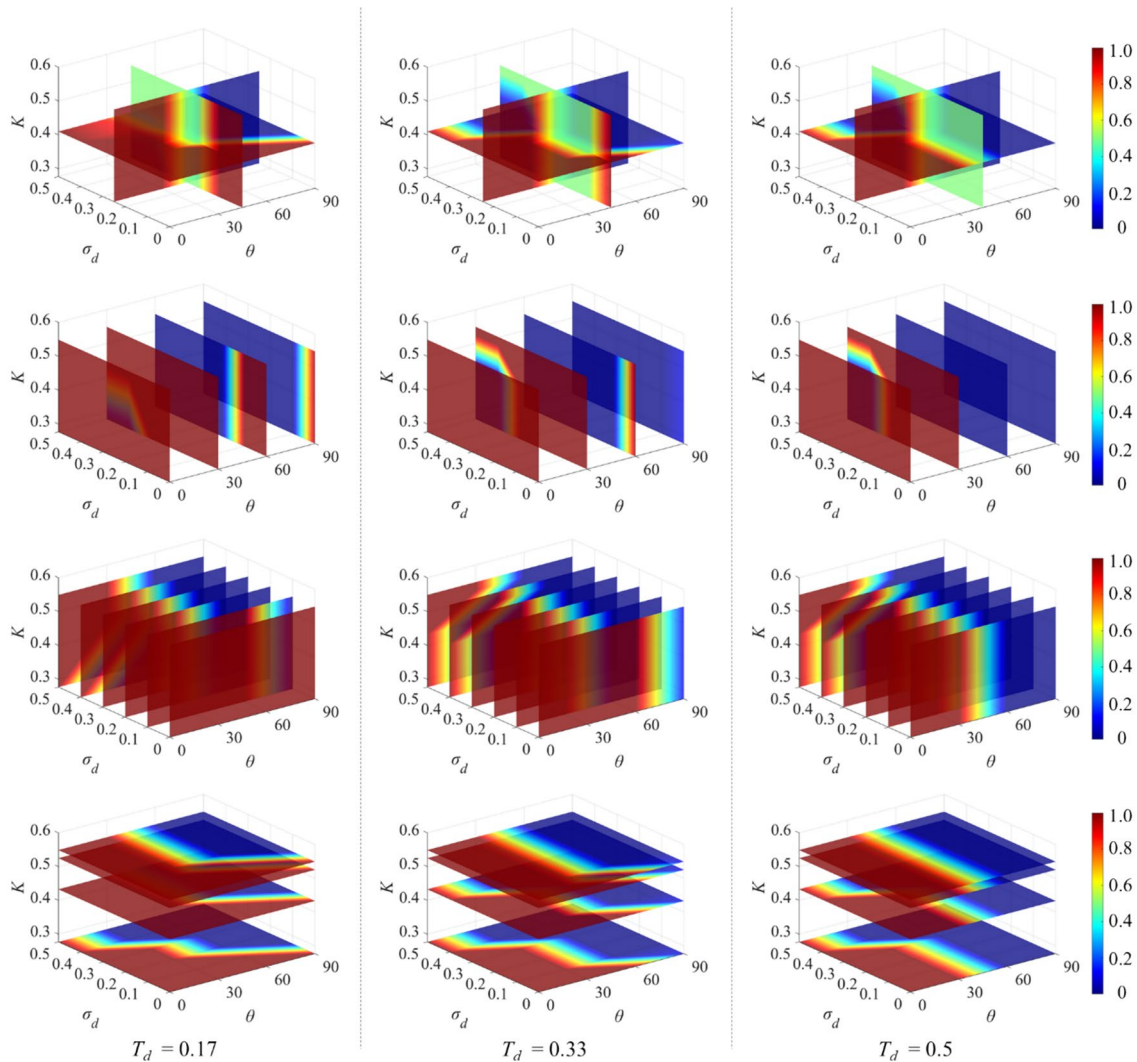


**Fig. 10** Three-dimensional interaction diagram of natural fractures and hydraulic fractures with different dimensionless nature fracture tensile strength coefficient (Color bar: 1 represents the opening of a natural fracture, 0 represents the crossing a natural fracture)



## 4 Discussion

### 4.1 Three-Dimensional Interaction Diagram Based on the Dimensionless Parameter

The above diagrams of the interaction between the hydraulic fracture and the natural fracture are only a part of the simulation results, and a total of 24 two-dimensional drawings are needed to fully display the simulation results. Diagrams of the interactions between the hydraulic fracture and the natural fracture will change with rock mechanical properties and pumping parameters. Therefore, to simplify the drawing charts and apply them universally, the dimensionless toughness coefficient  $K$  in Eq. 1, the dimensionless horizontal stress difference coefficient  $\sigma_d$  ( $\sigma_d = \Delta\sigma / \sigma_h$ ) and the dimensionless nature fracture tensile strength coefficient  $T_d$  ( $T_d = T_n / \sigma_t$ ) are introduced to describe the interaction between the hydraulic fracture and the natural fracture. Then, three sets of comprehensive maps with four parameters are finally formed via interpolation on the above two-dimensional maps. The query results shown in Fig. 10 are more convenient and help improve the level and efficiency of the reservoir stimulation design. Figure 10 shows that the interaction between natural fractures and hydraulic

fractures is dominated by geological conditions, and the geological range for complex hydraulic fractures is narrow. For example, when the natural fracture angle is less than  $30^\circ$  (more than  $60^\circ$ ) and the dimensionless horizontal stress difference coefficient  $\sigma_d$  is less than 0.4 (more than 0.4), the natural fractures keep opening (closing) and are not affected by engineering factors. On the other hand, the engineering parameters (dimensionless toughness coefficient) can affect the location and range of the strip to a certain extent. Therefore, not all reservoirs with a natural fracture distribution can realize complex fracture morphologies via massive hydraulic fracturing.

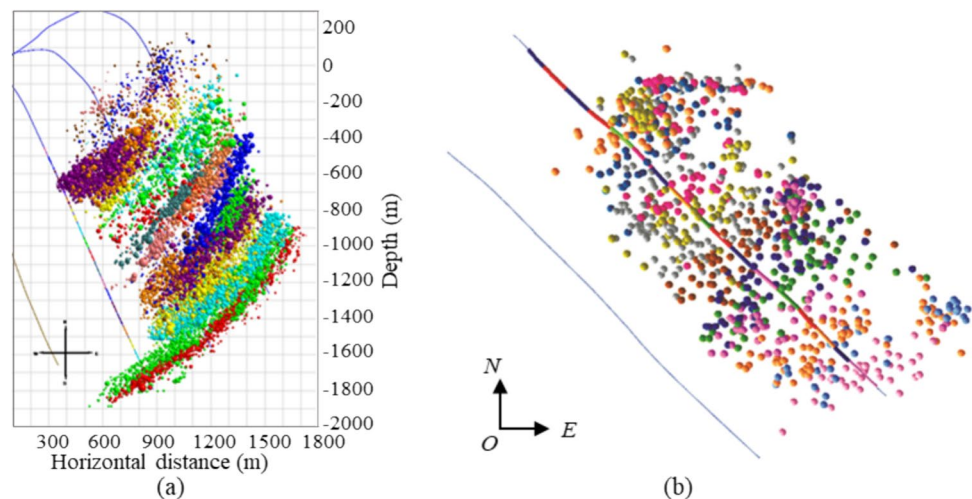
### 4.2 Application of a Three-Dimensional Interaction Diagram in Field Fracturing

Most unconventional oil and gas reservoirs in China have high horizontal stress differences (more than 3 MPa), as shown in Table 4, and there are both reservoirs with natural fractures and reservoirs without natural fractures. Figure 11a shows the microseismic event of a well during hydraulic fracturing in the Zhaotong national shale gas demonstration zone, where natural fractures do not develop. The microseismic signals are distributed mainly in the direction

**Table 4** Distribution characteristics of stress and natural fractures in major unconventional oil and gas reservoirs in China

	Lithology	Degree of natural fracture development	Horizontal stress difference/MPa
Chang 7 member in Changqing Oilfield	Sandstone	Nondevelopment	3~7
Baikouquan formation in Mahu oilfield	Conglomerate	Nondevelopment	8
Lucaogou formation in Jimsar oilfield	Carbonate rock, clastic rock	Nondevelopment	10~22
Longmaxi formation in Sichuan basin	Shale	Local development	4~12
Q1 period in Jilin oilfield	Sandstone	Development	9~18

**Fig. 11** (a) Microseismic events recorded from the stimulation in the Zhaotong national shale gas demonstration zone. (b) diagram of downhole microseismic monitoring during the fracturing of the Longmaxi shale in the Weiyuan block (Liu 2016)



perpendicular to the wellbore and the signals between clusters are neatly distributed. Therefore, multi-hydraulic fractures that extend perpendicular to the direction of the maximum principal stress are formed during staged multi-cluster fracturing, and complex hydraulic fractures are not formed. In contrast, the microseismic signal distribution of Longmaxi shale fracturing in the Weiyuan block is irregular in Fig. 11b, that is, a complex natural fracture network is formed (Liu 2016). To enhance unconventional reservoir stimulation, multistage fracturing technology with short cluster spacing would be effective and promising. Therefore, the above interaction diagram (Fig. 10) and field data (Fig. 11) indicate that different fracturing measures are required to achieve oil and gas stimulation for different reservoir characteristics. For example, in view of the large stress difference and natural fracture development characteristics of shale gas in southern Sichuan, dense cutting fracturing technology with 55–63 m per stage length, 3–7 clusters per stage and 18–10 m cluster spacing, can be used for construction. Considering the characteristics of the small stress difference and undeveloped natural fractures in the Changqing oilfield, fracturing parameters of 4–6 clusters per stage and 13–9 m per cluster spacing can be used. The application of fracturing parameters in both cases resulted in significant improvements in the oil and gas production indicators. In addition, it should be noted that in field hydraulic fracturing, hydraulic fracture propagation is related not only to natural fractures and construction parameters but also to differences in rock physical properties and geological conditions.

## 5 Conclusion

- (1) Laboratory three-dimensional hydraulic fracturing simulation technology considering natural fractures is established. The quantitative characterization of the spatial distribution morphology and mechanical properties of natural fractures can also be realized.
- (2) On the basis of the finite element method, a heterogeneous and multiscale numerical model of hydraulic fracture propagation is established to reveal the interaction between hydraulic fracture and natural fracture. Fracturing simulations can be realized from the experimental scale to the field scale.
- (3) Through physical and numerical simulations, the interaction results of natural fractures and hydraulic fractures are defined, and the geological and engineering factors affecting the propagation of hydraulic fractures are quantitatively analysed. The results revealed three interaction modes, namely, natural fracture opening, shearing and passing through. In actual fracturing, a single mode or several mixed mode action modes may exist. Higher horizontal stress differences, natural fracture angles, tensile strengths of natural fractures and pumping parameters are conducive to crossing natural fractures.
- (4) A dimensionless stimulation factor (dimensionless toughness coefficient) is introduced to create three sets of comprehensive charts with four parameters, which helps improve the level and efficiency of the treatment optimization design. The results show that the interaction between natural fractures and hydraulic fractures is dominated by geological conditions. Most unconventional oil and gas reservoirs in China have high horizontal stress differences in two directions, which makes it difficult to create complex fractures. Therefore, multistage fracturing technology with short cluster spacing is effective and promising.

**Acknowledgements** The authors acknowledge the support provided by the National Natural Science Foundation of China (Grant No. 42372337, No. 52234003), National Science Fund for Excellent Young Scholars (Grant No. 52222402) and Natural Science Starting Project of SWPU (Grant No. 2022QHZ009).

**Funding** No funding was received for conducting this study.

**Data Availability** Data will be made available on request.

## Declarations

**Conflict of Interest** The authors declare no conflicts of interest.

## References

- Arash D-T, Olson JE (2011) Numerical modeling of multistranded hydraulic-fracture propagation: Accounting for the interaction between induced and natural fractures. *SPE J* 16:575–581. <https://doi.org/10.2118/124884-PA>
- Chen X, Zhao J, Li Y, Yan W, Zhang X (2019) Numerical simulation of simultaneous hydraulic fracture growth within a rock layer: implications for stimulation of low-permeability reservoirs. *J Geophys Res Solid Earth* 124:13227–13249. <https://doi.org/10.1029/2019JB017942>
- De Pater CJ, Cleary MP, Quinn TS, Barr DT, Johnson DE, Weijers L (1994) Experimental verification of dimensional analysis for hydraulic fracturing. *SPE Prod Facil* 9:230–238. <https://doi.org/10.2118/24994-pa>
- Detournay E (2016) Mechanics of hydraulic fractures. *Annu Rev Fluid Mech* 48:311–339. <https://doi.org/10.1146/annurev-fluid-010814-014736>
- Detournay E (2004) Propagation regimes of fluid-driven fractures in impermeable rocks. *Int J Geomech* 4:35–45. [https://doi.org/10.1061/\(ASCE\)1532-3641\(2004\)4:1\(35\)](https://doi.org/10.1061/(ASCE)1532-3641(2004)4:1(35))
- Dontsov, E. V., 2022a. Morphology of multiple constant height hydraulic fractures versus propagation regime. *Int. J. Numer. Anal. Methods Geomech.* 1–7. <https://doi.org/10.1002/nag.3335>
- Dontsov EV (2022b) Analysis of a constant height hydraulic fracture driven by a power-law fluid. *Rock Mech Bull* 1:100003. <https://doi.org/10.1016/j.rockmb.2022.100003>

- Dontsov, E. V., 2016. An approximate solution for a penny-shaped hydraulic fracture that accounts for fracture toughness, fluid viscosity and leak-off. *R. Soc. Open Sci.* 3. <https://doi.org/10.1098/rsos.160737>
- Fisher, M.K., Heinze, J.R., Harris, C.D., Davidson, B.M., Wright, C.A., Dunn, K.P., 2004. Optimizing horizontal completion techniques in the barnett shale using microseismic fracture mapping. *SPE Annu. Tech. Conf. Proc.* <https://doi.org/10.2118/90051-ms>
- Fisher MK, Wright CA, Davidson BM, Goodwin AK, Fielder EO, Buckler WS, Steinsberger NP (2005) Integrating fracture-mapping technologies to improve stimulations in the Barnett shale. *SPE Prod Facil* 20:85–93. <https://doi.org/10.2118/77441-PA>
- Fu H, Huang L, Zhang F, Xu Y, Cai B, Liang T, Wang X (2021) Effect of perforation technologies on the initiation and propagation of hydraulic fracture. *Chinese J Rock Mech Eng* 40:3163–3173
- Guo J, Zhao X, Zhu H, Zhang X, Pan R (2015) Numerical simulation of interaction of hydraulic fracture and natural fracture based on the cohesive zone finite element method. *J Nat Gas Sci Eng* 25:180–188. <https://doi.org/10.1016/j.jngse.2015.05.008>
- He R, Yang J, Li L, Yang Z, Chen W, Zeng J, Liao X, Huang L (2023) Investigating the simultaneous fracture propagation from multiple perforation clusters in horizontal wells using 3D block discrete element method. *Front Earth Sci* 11:1–19. <https://doi.org/10.3389/feart.2023.1115054>
- Hu W, Wei Y, Bao J (2018) Development of the theory and technology for low permeability reservoirs in China. *Pet Explor Dev* 45:685–697. [https://doi.org/10.1016/S1876-3804\(18\)30072-7](https://doi.org/10.1016/S1876-3804(18)30072-7)
- Huang L, Dontsov E, Fu H, Lei Y, Weng D, Zhang F (2022) Hydraulic fracture height growth in layered rocks : Perspective from DEM simulation of different propagation regimes. *Int J Solids Struct* 238:111395. <https://doi.org/10.1016/j.ijsolstr.2021.111395>
- Huang L, He R, Yang Z, Tan P, Chen W, Li X, Cao A (2023a) Exploring hydraulic fracture behavior in glutenite formation with strong heterogeneity and variable lithology based on DEM simulation. *Eng Fract Mech* 278:109020. <https://doi.org/10.1016/j.engfractmech.2022.109020>
- Huang, L., Liao, X., Fan, M., Wu, S., Tan, P., Yang, L., 2024. Experimental and numerical simulation technique for hydraulic fracturing of shale formations. *Adv. Geo-Energy Res.* 13, 83–88. <https://doi.org/10.46690/ager.2024.08.02>
- Huang L, Liu J, Ji Y, Gong X, Qin L (2018) A review of multiscale expansion of low permeability reservoir cracks. *Petroleum* 4:115–125. <https://doi.org/10.1016/j.petlm.2017.09.002>
- Huang L, Liu J, Zhang F, Dontsov E, Damjanac B (2019) Exploring the influence of rock inherent heterogeneity and grain size on hydraulic fracturing using discrete element modeling. *Int J Solids Struct* 176:207–220. <https://doi.org/10.1016/j.ijsolstr.2019.06.018>
- Huang L, Liu J, Zhang F, Fu H, Zhu H, Damjanac B (2020) 3D lattice modeling of hydraulic fracture initiation and near-wellbore propagation for different perforation models. *J Pet Sci Eng* 191:107169. <https://doi.org/10.1016/j.petrol.2020.107169>
- Huang L, Tan J, Fu H, Liu J, Chen X, Liao X, Wang X, Wang C (2023b) The non-plane initiation and propagation mechanism of multiple hydraulic fractures in tight reservoirs considering stress shadow effects. *Eng Fract Mech* 292:109570. <https://doi.org/10.1016/j.engfracmech.2023.109570>
- Ishibashi T, Asanuma H, Mukuhira Y, Watanabe N (2023) Laboratory hydraulic shearing of granitic fractures with surface roughness under stress states of EGS: Permeability changes and energy balance. *Int J Rock Mech Min Sci* 170:105512. <https://doi.org/10.1016/j.ijrmms.2023.105512>
- Li M, Zhou D, Su Y (2023) Simulation of fully coupled hydro-mechanical behavior based on an analogy between hydraulic fracturing and heat conduction. *Comput Geotech* 156:105259. <https://doi.org/10.1016/j.compgeo.2023.105259>
- Liu Q, Li J, Liang B, Liu J, Sun W, He J, Lei Y (2023) Complex wettability behavior triggering mechanism on imbibition: a model construction and comparative study based on analysis at multiple scales. *Energy* 275:127434. <https://doi.org/10.1016/j.energy.2023.127434>
- Liu X (2016) Shale-gas well test analysis and evaluation after hydraulic fracturing by stimulated reservoir volume (SRV). *Nat Gas Ind B* 3:577–584. <https://doi.org/10.1016/j.ngib.2017.05.008>
- Li Y, Peng G, Du T, Jiang L, Kong X (2024a) Advancing fractured geothermal system modeling with artificial neural network and bidirectional gated recurrent unit. *Appl Energy* 372:123826. <https://doi.org/10.1016/j.apenergy.2024.123826>
- Li Y, Jiang X, Tang J, Liu B (2024b) Simulation study of acid fracturing initiation with consideration of rock mechanics parameter variations. *Rock Mech Rock Eng.* <https://doi.org/10.1007/s00603-024-03809-6>
- Li Y, Long M, Tang J, Chen M, Fu X (2020) A hydraulic fracture height mathematical model considering the influence of plastic region at fracture tip. *Pet Explor Dev* 47(1):184–195. [https://doi.org/10.1016/S1876-3804\(20\)60017-9](https://doi.org/10.1016/S1876-3804(20)60017-9)
- Llanos EM, Jeffrey RG, Hillis R, Zhang X (2017) Hydraulic fracture propagation through an orthogonal discontinuity: a laboratory, analytical and numerical study. *Rock Mech Rock Eng* 50:2101–2118. <https://doi.org/10.1007/s00603-017-1213-3>
- Luo H, Xie J, Huang L, Wu J, Shi X, Bai Y, Fu H, Pan B (2022) Multi-scale sensitivity analysis of hydraulic fracturing parameters based on dimensionless analysis method. *Lithosphere* 2022:9708300. <https://doi.org/10.2113/2022/9708300/5633720/9708300.pdf>
- Mao R, Feng Z, Liu Z, Zhao Y (2017) Laboratory hydraulic fracturing test on large-scale pre-cracked granite specimens. *J Nat Gas Sci Eng* 44:278–286. <https://doi.org/10.1016/j.jngse.2017.03.037>
- Niu Q, Cao L, Sang S, Wang W, Zhou X, Yuan W, Ji Z, Chang J, Li M (2021) Experimental study on the softening effect and mechanism of anthracite with CO<sub>2</sub> injection. *Int J Rock Mech Min Sci* 138:104614. <https://doi.org/10.1016/j.ijrmms.2021.104614>
- Niu Q, Wang Q, Wang W, Chang J, Chen M, Wang H, Cai N, Fan L (2022) Responses of multi-scale microstructures, physical-mechanical and hydraulic characteristics of roof rocks caused by the supercritical CO<sub>2</sub>-water-rock reaction. *Energy* 238:121727. <https://doi.org/10.1016/j.energy.2021.121727>
- Pidho JJ, Liang Y, Cheng Y, Yan C (2023) Analysis of interaction of hydraulic fractures with natural fractures and bedding planes in layered formation through cohesive zone modelling. *Theor Appl Fract Mech* 123:103708. <https://doi.org/10.1016/j.tafmec.2022.103708>
- Song R, Liu J, Cui M (2017) A new method to reconstruct structured mesh model from micro-computed tomography images of porous media and its application. *Int J Heat Mass Transf* 109:705–715. <https://doi.org/10.1016/j.ijheatmasstransfer.2017.02.053>
- Song R, Wang Y, Ishutov S, Zambrano-Narvaez G, Hodder KJ, Chalaturnyk RJ, Sun S, Liu J, Gamage RP (2020) A Comprehensive Experimental Study on Mechanical Behavior, Microstructure and Transport Properties of 3D-printed Rock Analogs. *Rock Mech Rock Eng* 53:5745–5765. <https://doi.org/10.1007/s00603-020-02239-4>
- Tan P, Chen Z, Fu S, Zhao Q (2023) Experimental investigation on fracture growth for integrated hydraulic fracturing in multiple gas bearing formations. *Geoenergy Sci Eng* 231:212316. <https://doi.org/10.1016/j.geoen.2023.212316>
- Tan P, Jin Y, Pang H (2021) Hydraulic fracture vertical propagation behavior in transversely isotropic layered shale formation with transition zone using XFEM-based CZM method. *Eng Fract Mech* 248:107707. <https://doi.org/10.1016/j.engfracmech.2021.107707>
- Tan P, Chen Z, Huang L, Zhao Q, Shao S (2024a) Evaluation of the combined influence of geological layer property and in-situ

- stresses on fracture height growth for layered formations. *Pet Sci*. <https://doi.org/10.1016/j.petsci.2024.07.014>
- Tan P, Fu S, Huang L, Chen Z, Cao J (2024b) Effects of orthogonal cleat structures on hydraulic fracture evolution behavior. *Geoenery Sci Eng* 241:213119. <https://doi.org/10.1016/j.geoen.2024.213119>
- Warpinski NR, Lorenz JC, Branagan PT, Myal FR, Gall BL (1993) Examination of a cored hydraulic fracture in a deep gas well. *SPE Prod Facil* 8:150–158. <https://doi.org/10.2118/22876-pa>
- Warpinski NR, Teufel LW (1987) Influence of Geologic Discontinuities on Hydraulic Fracture Propagation. *JPT. J Pet Technol* 39:209–220. <https://doi.org/10.2118/13224-pa>
- Weng, X., Kresse, O., Cohen, C., Wu, R., Gu, H., 2011. Modeling of hydraulic fracture network propagation in a naturally fractured formation. *Soc. Pet. Eng. - SPE Hydraul. Fract. Technol. Conf.* 2011 i, 298–315. <https://doi.org/10.2118/140253-ms>
- Wu M, Jiang C, Song R, Liu J, Li M, Liu B, Shi D, Zhu Z, Deng B (2023) Comparative study on hydraulic fracturing using different discrete fracture network modeling: Insight from homogeneous to heterogeneity reservoirs. *Eng Fract Mech* 284:109274. <https://doi.org/10.1016/j.engfracmech.2023.109274>
- Zhang F, Damjanac B, Maxwell S (2019) Investigating hydraulic fracturing complexity in naturally fractured rock masses using fully coupled multiscale numerical modeling. *Rock Mech Rock Eng* 52:5137–5160. <https://doi.org/10.1007/s00603-019-01851-3>
- Zhang F, Huang L, Yang L, Dontsov E, Weng D (2022a) Numerical investigation on the effect of depletion-induced stress reorientation on infill well hydraulic fracture propagation. *Pet Sci* 19:296–308. <https://doi.org/10.1016/j.petsci.2021.09.014>
- Zhang F, Mack M (2017) Integrating fully coupled geomechanical modeling with microseismicity for the analysis of refracturing treatment. *J Nat Gas Sci Eng* 46:16–25. <https://doi.org/10.1016/j.jngse.2017.07.008>
- Zhang JN, Yu H, Xu WL, Lv CS, Micheal M, Shi F, Wu HA (2022b) A hybrid numerical approach for hydraulic fracturing in a naturally fractured formation combining the XFEM and phase-field model. *Eng Fract Mech* 271:108621. <https://doi.org/10.1016/j.engfracmech.2022.108621>
- Zhang R, Zhao C, Yang C, Xing J, Morita C (2021) A comprehensive study of single-flawed granite hydraulically fracturing with laboratory experiments and flat-jointed bonded particle modeling. *Comput Geotech* 140:104440. <https://doi.org/10.1016/j.compgeo.2021.104440>
- Zhang X, Jeffrey RG, Thiercelin M (2007) Deflection and propagation of fluid-driven fractures at frictional bedding interfaces: A numerical investigation. *J Struct Geol* 29:396–410. <https://doi.org/10.1016/j.jsg.2006.09.013>
- Zhang X, Wu B, Jeffrey RG, Connell LD, Zhang G (2017) A pseudo-3D model for hydraulic fracture growth in a layered rock. *Int J Solids Struct* 115:208–223. <https://doi.org/10.1016/j.ijsolstr.2017.03.022>
- Zhang Y, Long A, Zhao Y, Wang C, Wu S, Huang H (2023) Impacts of wellbore orientation with respect to bedding inclination and injection rate on laboratory hydraulic fracturing characteristics of Lushan shale. *Fuel* 353:129220. <https://doi.org/10.1016/j.fuel.2023.129220>
- Zheng Y, He R, Huang L, Bai Y, Wang C, Chen W (2022) Exploring the effect of engineering parameters on the penetration of hydraulic fractures through bedding planes in different propagation regimes. *Comput Geotech* 146:104736. <https://doi.org/10.1016/j.compgeo.2022.104736>

**Publisher's Note** Springer Nature remains neutral with regard to jurisdictional claims in published maps and institutional affiliations.

Springer Nature or its licensor (e.g. a society or other partner) holds exclusive rights to this article under a publishing agreement with the author(s) or other rightsholder(s); author self-archiving of the accepted manuscript version of this article is solely governed by the terms of such publishing agreement and applicable law.